Journal of Catalysis **206,** 188–201 (2002)
doi:10.1006/jcat.2001.3485, available online at http://www.idealibrary.com on IDEAL®

Heptane Reforming over Pt–Re/Al_2O_3: Reaction Network, Kinetics, and Apparent Selective Catalyst Deactivation

K. Liu,*,†,[1] S. C. Fung,† T. C. Ho,† and D. S. Rumschitzki*,[2]

*Department of Chemical Engineering, City College of the City University of New York, and GSUC–CUNY, New York, New York 10031; and †Corporate Strategic Research Lab., ExxonMobil Research and Engineering Co., Annandale, New Jersey 08801

Received May 11, 2001; revised November 28, 2001; accepted November 28, 2001

This is a continuation of our previous work aimed at developing a fundamental, *a priori* model for predicting how a reforming catalyst deactivates in a fixed-bed reactor due to coke formation. Specifically, we construct a lumped reaction network for *n*-heptane reforming on a bifunctional Pt–Re/Al_2O_3 catalyst using both differential and integral rate data. The data are obtained from a vibrational microbalance and a multioutlet fixed-bed reactor with *n*-heptane or reaction intermediates as the feed. The network, including a five-membered naphthene lump that is the primary coke precursor, has a minimum number of reactions and corresponding adjustable rate parameters, almost all of which are individually determined by targeted experiments. The resulting kinetic model, coupled with a previously developed catalyst coking kinetic model, correctly predicts the long-term spatiotemporal behavior of product composition and coke-on-catalyst for a fixed-bed reformer. The results strongly suggest the need to partition the reforming reactions into two subgroups: those that are significantly affected by coke and those that are not. The approach taken here, which provides both fundamental insights and a quantitative basis for improving catalysts and processes, can also be extended to other catalytic systems.

INTRODUCTION

In our previous paper (1), we assembled a preponderance of experimental evidence that five-membered naphthenes (C5N) are the major coke precursors in *n*-heptane reforming over an unsulfided Pt–Re/Al_2O_3 catalyst under conditions close to those of a commercial reformer. If one accepts the weight of this evidence and would like to predict coke profiles in operating reformers, it is absolutely necessary to have at one's disposal a lumped reaction network for *n*-heptane reforming that is simple, robust, and contains C5N as one of its lumps. Moreover, such a model will be useful for gaining a quantitative understanding of the catalyst deactivation process. We have reported (2) a coking kinetics model based on vibrational microbalance experiments with a feed whose only hydrocarbon constituent is the coke precursor. Thus, once armed with a reaction kinetics model, we can combine it with the coking kinetics model to better understand and predict reformer performance over coking time scales, on the one hand, and to predict the bed's coke profile based on the precursor's dynamic profile, on the other. This is the subject of this study.

Specifically, the present study consists of two parts. The first part addresses the reforming kinetics. We operate the microbalance in differential mode to probe the relative importance of individual lumped reactions, which helps eliminate kinetically insignificant reaction pathways. Once a network emerges as the leading candidate, the microbalance further gives fairly tight estimates of the rate constants for selected subsets of the network by using the reaction intermediates as the feed. The remaining data are amassed in an integral multioutlet fixed-bed reactor. These data allow estimation and testing of the remaining rate constants by using the already determined reaction paths and rate constants. The resulting kinetic model has very few adjustable parameters. The second part combines the reforming kinetics model with previously developed coking kinetics to predict the development of reactor coke profiles and the evolution of product composition throughout the lifetime of the catalyst. The agreement between theory and experiment is excellent. A significant result suggested by this modeling study is that the damaging effect of coke-on-catalyst may be quite selective in that some reactions appear to be more sensitive to coke than others. And the data suggest that the deactivation process is primarily governed by certain metal sites that are most vulnerable to coke deposition. Such a selective deactivation phenomenon would have strong implications for catalyst design and process development and optimization.

The paper's layout consists of an overview of prior work on reforming kinetics, followed by experimental determination of reforming kinetics and lastly by the construction of an *a priori* reactor model that ties reforming and catalyst coking deactivation together.

[1] Current address: International Fuel Cells, United Technologies Corp., 195 Governor's Highway South Windsor, CT 06074.

[2] To whom correspondence should be addressed.

0021-9517/02 $35.00

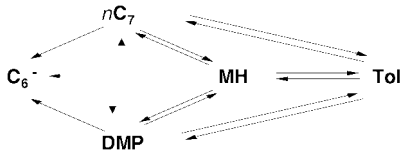

SCHEME 1. C_6^-, cracking products; DMP, dimethylpentane + 3-ethylpentane; MH, methylhexane; nC_7, *n*-heptane; Tol, toluene.

LITERATURE ON REFORMING KINETICS

Kugelmans (3), McHenry *et al.* (4), and Mahoney (5) proposed reaction networks for *n*-heptane reforming over the Pt/Al_2O_3 catalyst. Surprisingly, though, there have been relatively few attempts to determine the kinetics of *n*-heptane reforming over the more industrially relevant $Pt–Re/Al_2O_3$ catalyst. Clem (6) proposed a reaction scheme as a basis for a kinetics model of the *n*-heptane reforming for both $Pt–Re/Al_2O_3$ and Pt/Al_2O_3 catalysts (see Scheme 1). The model contains 14 parameters because it considers all possible reversible reactions in the network.

Van Trimpont *et al*. (7–9) studied *n*-heptane reforming kinetics over both Pt/Al_2O_3 and $Pt–Re/Al_2O_3$ catalysts for the range of 627–776°K, 440–1650 kPa, and 400–1550 kPa H_2 partial pressures. They neglected direct dehydrocyclization and cracking of *n*-heptane. Sun *et al.* (10, 11) reached a similar conclusion for the $Pt–Sn/Al_2O_3$ catalyst in the temperature and pressure ranges of 733–773°K and 800–1200 kPa. Ramage *et al.* (12, 13) developed a reforming kinetics model for industrial feedstocks. In Scheme 2, neglecting the C_8 fraction, we show their lumped reforming network for C_7 hydrocarbons. Since normal paraffins and isoparaffins give significantly different octane numbers, Sun *et al.* (10, 11) segregated these into two distinct species lumps.

From the foregoing literature review, one sees that there are significant discrepancies among the published reaction networks for nC_7 reforming. In this study, we obtain both differential and integral rate data using *n*-heptane and reaction intermediates as the feeds. The resulting kinetics model, while consistent with these data and with thermodynamics, also passes the stringent test that it correctly predicts the reactor coke profile as functions of on-stream time.

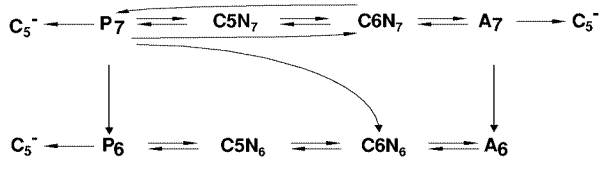

SCHEME 2. A, aromatics; C_5^-, cracking products; $C5N_6$, methylcyclopetanes; $C6N_6$, cyclohexane; P, paraffins.

EXPERIMENTAL

Reactors and Procedures

We employed a novel vibrational microbalance (1) and a multioutlet integral reactor for the present kinetics studies. The latter reactor has four outlets along its wall, which allows us to take one gas sample at a time through a stream selection valve. In this way one can amass conversion–space time data for the kinetics analysis by either changing the catalyst loading in different sections or varying the feed rates, or both. Since the sample stream extracts less than 5% of the total volumetric flow traversing the catalyst bed, there is little change in the space velocity due to the diversion of the sample stream. The multioutlet reactor system has been described in detail elsewhere (1, 14).

A three-zone furnace with independent temperature controllers provides varying heat input to different sections of the reactor to facilitate isothermal operation. Also, dilution of the catalyst (1.6-mm extrudates) with inert, randomly shaped quartz particles with an average diameter of 1.0 mm is necessary to avoid axial temperature gradients that would otherwise result from the highly endothermic aromatization reaction. These measures give essentially a uniform temperature profile along the 33-cm reactor. A typical run's loading consists of a total of 5 g of catalyst, diluted with quartz particles, in the four catalyst sections above outlet 4. Table 1 shows the different loadings of the catalyst in the reactor's four sections and the corresponding space velocities. The amount of catalyst above outlet 1 is labeled Section 1; the catalyst between outlets 1 and 2 is Section 2, and so on. A $\frac{1}{2}$-in. section of quartz particles separates the sections from each other to avoid ambiguity in the amount of catalyst attributed to each section. We vary the conversion either by changing the feed rate for a given catalyst loading distribution or by changing the catalyst loading of different sections for a given feed rate. The reforming conditions for *n*-heptane on the $Pt–Re/A1_2O_3$ catalyst are similar to those in commercial units. Specifically, temperatures are 733, 750, 772, 783, and 794°K at 517 kPa. At each temperature, three runs totaling 12 liquid-weight hourly-space velocities (WHSVs) constitute the kinetics data. Experiments at 207, 345, 517, and 1034 kPa at 750°K provide the total pressure dependence of the kinetics. To keep the number of manipulated variables small, we fix the hydrogen-to-hydrocarbon mole ratio in all experiments at 3, a value typical of commercial operation.

The procedures used for catalyst pretreatment appear in detail in (14) and a summary follows: After loading, one heats the catalyst from room temperature to 789° at 3°K/min under 2000 ml/min (at ambient conditions) of H_2 and maintains this temperature for 8 h to reduce the catalyst *in situ*. A gradual, 3-h cooling of the reactor to 643°K then precedes the introduction of the *n*-heptane

TABLE 1

Catalyst Loading and Corresponding Space Velocities of Different Sections

Run	Section 1				Section 2				Section 3			
Outlet number	4	3	2	1	4	3	2	1	4	3	2	1
WHSV (g/h-g catalyst)	2	4	10	110	6	14	26	120	8	18	57	133
Catalyst loading (g)	2.5	1.5	0.91	0.09	2.85	1.0	0.9	0.25	2.8	1.5	0.4	0.3

reactor feed. A subsequent slow, 3-h heating of the reactor brings it to run temperature. On-stream time begins the moment the reactor attains a preselected temperature. A rotating selection valve directs the reaction products from each of the outlets to an HP5880 GC equipped with a 50-m capillary column coated with cross-linked methylsilicone gum.

At the end of the run the liquid feed is stopped, and the reactor is cooled to 643°K over 3 h and maintained at this temperature for 5 h in hydrogen flowing at 430 ml/min (at ambient conditions). This procedure strips the reversibly adsorbed hydrocarbons off the catalyst, so as not to contribute to the temperature-programmed oxidation (TPO) signal during the analysis of the catalyst coke. Following the 643°K hydrogen stripping, the reactor is cooled to room temperature under flowing hydrogen.

Certain preliminary studies are necessary before beginning the bulk of the experimental work. Tests with various mass velocities under otherwise identical reaction conditions reveal no external mass transfer limitations. Tests with different sizes of catalyst particles under otherwise constant conditions to check for pore diffusion limitations show a minimal effect of particle size. This is consistent with our estimated effectiveness factor of about 0.9 for 1.6-mm extrudates at 772°K.

Catalytic reforming reactions often undergo very significant and rapid changes during the start-up period. Under our operating conditions, the catalyst essentially lines out its activity within ~30 h. It is generally accepted that the rapid formation of an initial coke level on the catalyst is responsible for this catalyst "lineout" or "equilibration." Clearly, a systematic kinetics study of the effects of space velocity, temperature, pressure, or some other process variable would be difficult in the rapidly changing period of the catalyst itself. Despite the fact that the catalyst continues to change during its life, its rate of change slows significantly to a time scale that is long compared to reforming reaction times after this lineout period. One can thus complete an isolated experimental study of reforming kinetics without considering catalyst deactivation over a narrow time window (<10 h) after the lineout period. In our work, we start each run with fresh catalyst and continue anywhere from 80 to 250 h. With such long experiments, we can clearly distinguish the lineout period from the long-term catalyst deactivation and thus safely identify the postlineout period. In most cases, the data between 30 and 40 h are used for evaluating kinetics parameters.

After terminating the run, we discharge the catalyst in discrete sections without mixing so as to be able to measure the coke content of each section by TPO. Fung and Querini (15) have detailed the TPO technique. References (1) and (2) detail the procedures for measuring reactor coke profiles in the multioutlet fixed bed reactor.

As mentioned, in addition to the multioutlet integral reactor, we run the vibrational microbalance as a differential reactor and check the existence and importance of each individual reaction by feeding different hydrocarbons (reactants, intermediates, and final products) to the microbalance at WHSV = 30–80, H_2/hydrocarbon molar ratio = 3, 750°K, 30 psi, with 0.1 g of catalyst loaded. Without going into great detail (1), we note that, in contrast to traditional thermogravimetric balances, all of the feed passes through the catalyst bed in the vibrational microbalance, thereby determining the true space time over the catalyst. Moreover, the gas concentrations that the differential bed sees are essentially directly measured.

Materials

The gases used in this research are cylinder hydrogen of electrolytic grade (99.95%), cylinder helium (99.95%), and cylinder nitrogen (99.95%). The liquid feed, *n*-heptane (nC_7), methylcyclopentane (MCP), ethylcyclopentane (ECP), and 2-methylhexane (2MH) are all analytic pure grade (99 mol%). The bimetallic Pt–Re/Al_2O_3 catalyst, in the form of $\frac{1}{16}$-in. extrudate in the reactor, contains 0.3 wt% Pt, 0.3% wt% Re, and 0.9 wt% Cl and has a BET specific surface area of 200 m^2/g. We neither presulfide the catalyst nor add sulfur to the feed during the run. Catalyst particle sizes are 177–250 μm in the microbalance experiments.

KINETICS MODEL

Our first task here is to implement an experimental program to adequately justify an appropriate reaction network that contains C5 naphthene as a single lump. Perhaps a safe way to do this, i.e., to investigate the reaction paths that compose the reaction network over a wide range of conversions, is to use two reactor systems. One is the microbalance used as a differential reactor primarily for testing the existence and importance of individual reactions.

The other is the multioutlet integral reactor for procuring high-conversion data typical of commercial operation.

Basic Species, Lumps, and Kinetic Trends

The major products of nC_7 reforming are toluene, iC_7 (branched heptanes), and cracking products (C_1–C_6). Due to the importance of the C5N contribution to coke formation (2), it is advantageous to segregate out all of the C5 naphthenes as a separate lump, even though this lump's concentration is much lower than that of other lumps. Recall that the reaction and deactivation essentially decouple after the initial ~30-h lineout, since the time scale of catalyst deactivation becomes much longer than that of the main reactions. We use only the concentration data after ~30 h and within a narrow time window of less than 10 h in estimating the reforming kinetics parameters. As will be discussed later, the long-term behavior of the catalyst is accounted for through a deactivation function determined previously (2). As illustrative examples, Figs. 1 and 2 plot reactant and product concentrations versus space time for 750 and 772°K at an on-stream time of 30–40 h and 517 kPa. (The solid curves are model predictions to be discussed later.) Both the iC_7 and the C5N lumps show maxima, indicating that they are reaction intermediates. The toluene (Tol) and lighter hydrocarbon (C_1–C_6) yields increase monotonically with space time, indicating that they are end products. After 10 min of space time, iC_7 and nC_7 decline concurrently and their ratio remains fairly constant, which, along with the fact that the iC_7s themselves are roughly in an equilibrium distribution, suggests that their interconversion reactions may be much faster than all other interlump reactions at these space times.

In kinetics studies, after postulating a reaction network, one often estimates all of the rate parameters from the comparison of the integrated model equations with experimental data using the reactant (i.e., *n*-heptane in our case) as the feed. Such a method can be very insensitive to changes in network structure and for a particular network can lead to more than one set of parameters that give equally good fits. Moreover, it is well known that the requirement that a multistep model kinetically describes the data from a particular experiment can tightly constrain certain parameter values while remaining extremely insensitive to variations in other parameter values. Rather, a proper parameter estimation procedure requires experiments using multiple feeds including reactants, reaction intermediates, and products. Each experiment is designed to make its result sensitive to a particular parameter or to a small subset of the parameters. It is then critical to subject rate constants derived in this way to some consistency checks, e.g., to see if they are consistent with physicochemical laws and thermodynamics (more on this later).

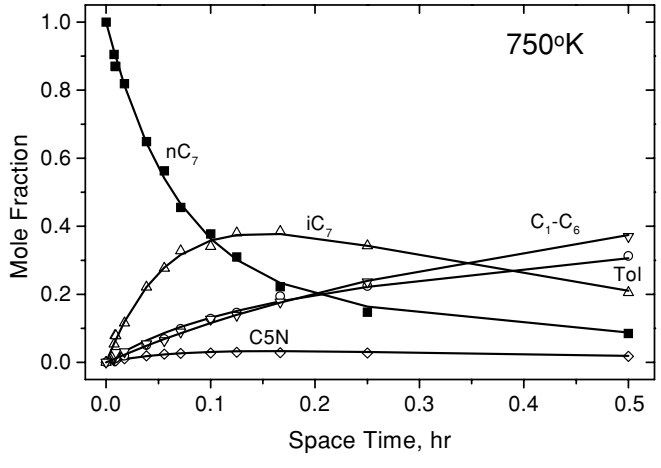

FIG. 1. Concentration versus space time data obtained from the multioutlet fixed-bed reactor, 750°K, 517 kPa. Model (—) prediction, k_6 and k_7, determined in microbalance with ECP.

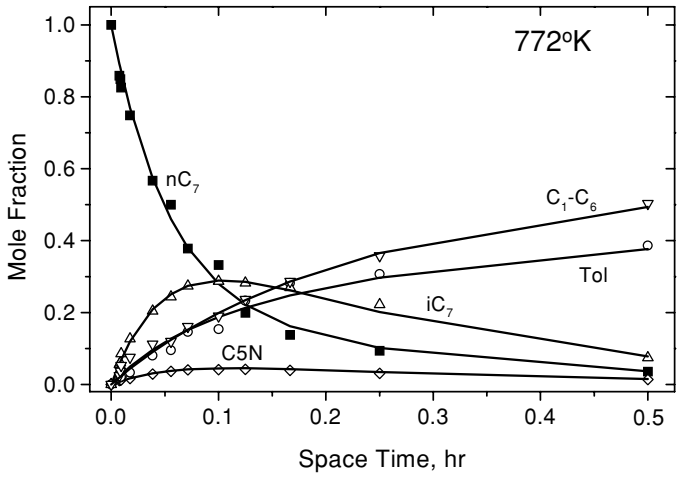

FIG. 2. Concentration versus space time data obtained from the multioutlet fixed-bed reactor, 772°K, 517 kPa. Model (—) prediction, k_6 and k_7, determined in microbalance with ECP.

Thus we examine the reaction networks proposed in the following and perform specific experiments that target individual component reactions. Each experiment attempts to ascertain whether a chemically plausible reaction occurs at a relevant rate and if so, what its rate constant is. Only after doing a number of such investigations do we examine the integral data for nC_7 feed to determine the parameters not easily accessible by this direct method.

For example, Clem's model (6) mentioned previously contains 14 reactions, because it allows almost all possible (reversible) reactions between lumps. By feeding pure toluene and hydrogen to the microbalance, one can test whether toluene reacts to nC_7 or to iC_7. The result (data not shown) shows that toluene is virtually unreactive at 750°K, 207 kPa, H_2/toluene molar ratio = 3, and 50 WHSV [g feed/(g catalyst · h)]. Thus, there are no significant reverse reactions from toluene to nC_7 and iC_7 under these conditions.

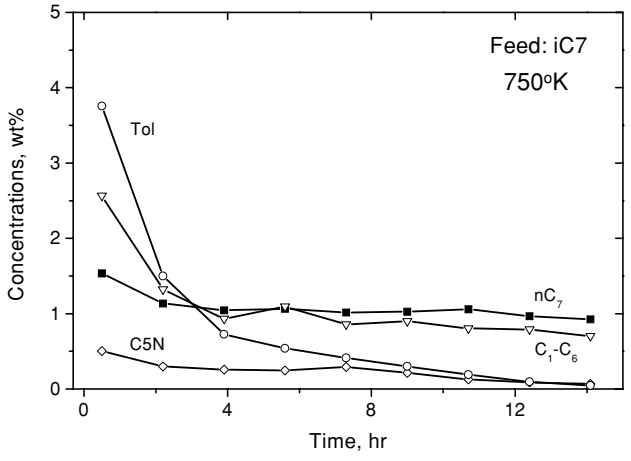

FIG. 3. Concentration versus on-stream time data obtained by feeding 2-methylhexane (iC_7) to the differential microbalance reactor at 750°K, 207 kPa, $H_2/iC_7 = 3$, and 80 WHSV.

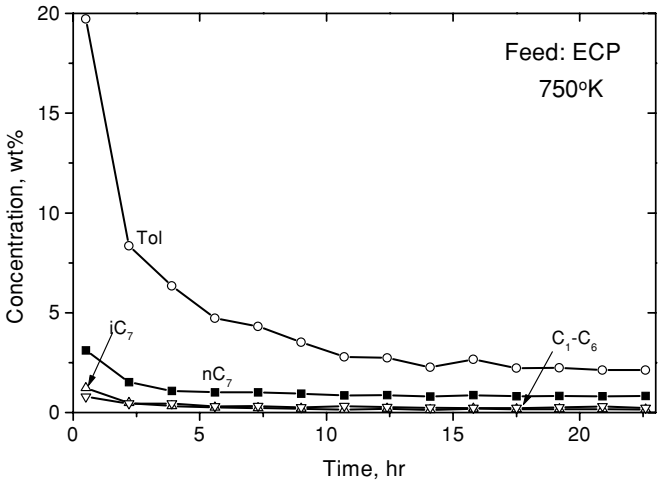

FIG. 5. Concentration versus on-stream time data obtained by feeding ethylcyclopentane to the differential microbalance reactor at 750°K, 207 kPa, $H_2/ECP = 3$, and 35 WHSV.

McHenry *et al.* (4) and Clem's (6) prior networks posit that a dehydrocyclization ring closure of nC_7 and iC_7 produces toluene directly and rapidly. To test this pathway for iC_7, we run the microbalance using 2-methylhexane, the major iC_7 formed in nC_7 reforming, as the feed at 750°K, 207 kPa, $H_2/iC_7 = 3$, and 80 WHSV. As Fig. 3 shows, after the initial catalyst transient period, the major products are nC_7 and cracking products. The near absence of toluene shows that ring closure of this iC_7 molecule is not important compared to that of nC_7. Moreover, the presence of significant cracking product without C5N or toluene suggests that iC_7 cracks directly, without an nC_7 intermediate and that the isomerization reaction, while fast, is not effectively instantaneous relative to cracking. Note that the ratio of the amounts of cracking product in Figs. 3 and 4 is approximately the inverse of the ratio of their WHSVs. Since the microbalance in this experiment is almost a differential reactor, this implies that the cracking rates of nC_7 and of iC_7 proceed at comparable rates.

When comparing Van Trimpont *et al.*'s model to that of Ramage *et al.* (12, 13), one should ask, is the dehydrocyclization reaction (i) a direct six-membered ring closure, (ii) a five-membered ring closure to cyclopentane intermediates (C5N) followed by ring expansion to cyclohexane, or (iii) a simultaneous six- and five-membered ring closure? To answer these questions, we feed pure ECP and MCP (Figs. 5 and 6) as model compounds of C5N to the microbalance reactor and measure the rate of ring expansion and ring opening in differential operation mode at 750°K and 207 kPa. Aromatics (toluene/benzene) and the normal paraffins (nC_7/nC_6) are the major products of ECP/MCP reforming. Cracking and isoparaffin formation rates are,

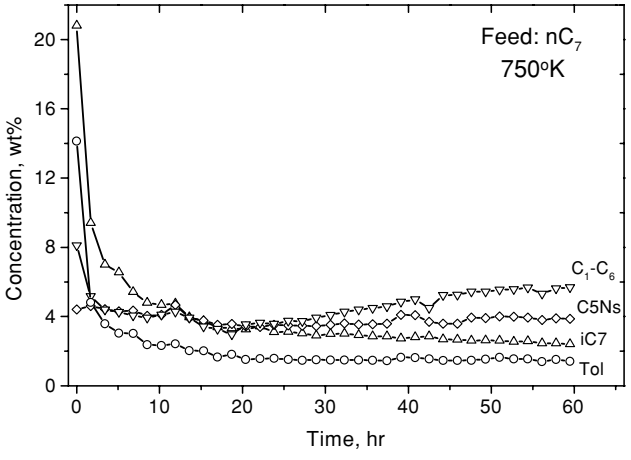

FIG. 4. Concentration versus on-stream time data obtained by feeding *n*-heptane to the differential microbalance reactor at 750°K, 207 kPa, $H_2/nC_7 = 3$, and 30 WHSV.

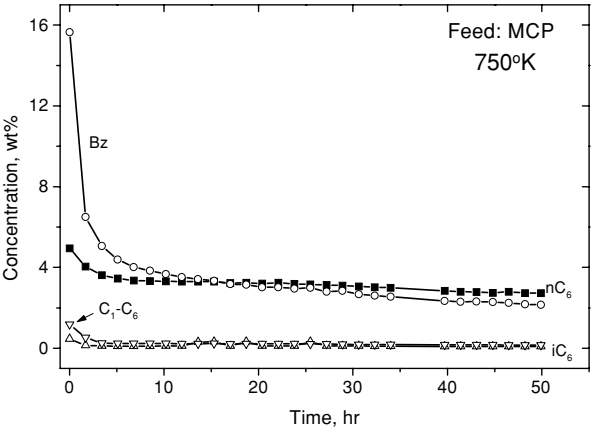

FIG. 6. Concentration versus on-stream data obtained by feeding methylcyclopentane to the differential microbalance reactor at 750°K, 207 kPa, $H_2/MCP = 3$, and 50 WHSV.

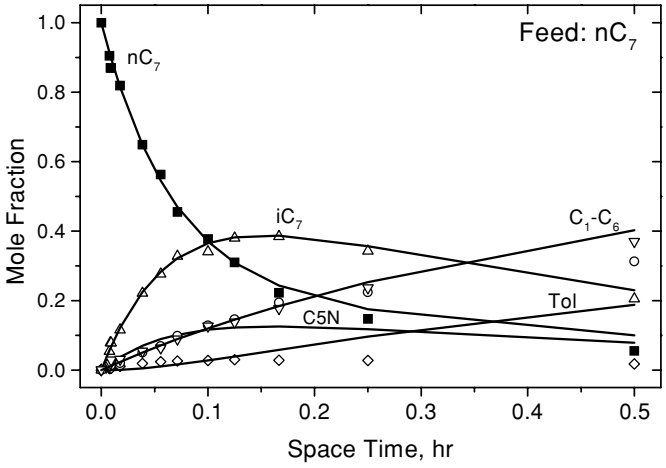

FIG. 7. Model prediction obtained by neglecting direct dehydrocyclization of nC_7, 750°K, 517 kPa. Model (—) fails to predict toluene and C5N concentrations.

by comparison, negligible after the initial transient period. In fact, they may even require an nC_7 intermediate. It is now a simple matter to calculate the rate constants for the C5N-to-toluene and C5N-to-nC_7 reactions from these data. Surprisingly the rate constant for C5N to toluene measured this way is much smaller than Van Trimpont *et al.*'s (7–9) value. This has some major consequences. Consider the integral reactor data for nC_7 feed in Fig. 7 (a blow-up version is shown in Fig. 8). After the initial catalyst transient, the reaction C5N → toluene, with the calculated rate constant, the C5N concentration shown in the figure and with no other parallel toluene formation pathway is incapable of producing anywhere near the amount of toluene observed. This suggests that in addition to five-membered ring closure, a simultaneous, direct six-membered ring dehydrocyclization also produces aromatics.

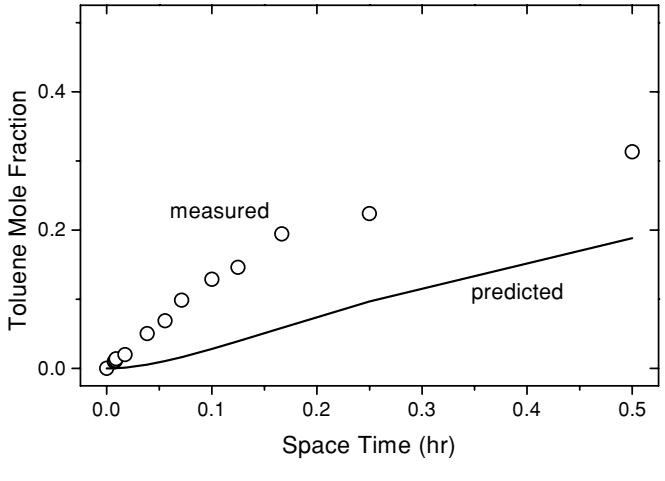

FIG. 8. Model prediction obtained by neglecting direct dehydrocyclization of nC_7 (blow-up version of Fig. 7); —, model prediction.

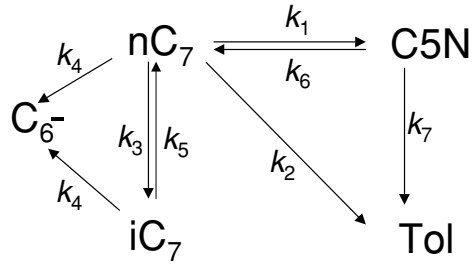

FIG. 9. Lumped reaction network for *n*-heptane reforming over unsulfided Pt–Re/Al_2O_3 catalyst.

Finally, we do not need to include a saturated six-membered naphthene lump explicitly in the nC_7 reforming kinetics scheme, because the dehydrogenation of methylcyclohexane to toluene is much faster than the other reactions in the network and its concentration is extremely low.

In summary, Fig. 9 shows the simplest lumped reaction network for nC_7 reforming that summarizes these targeted experiments from both the integral and the differential reactors.

Rate Equation and Parameter Estimation

Given the above lumped reaction network, the next step is to evaluate the model parameters. This also provides a test, albeit a weak one, of the network itself. Previous studies (6, 7–9, 13, 16) and our data show that when H_2 is present in large excess, all reactions in the network can be adequately treated as pseudo first order. Note that the reactor is practically isothermal. Despite the large excess of H_2, the net H_2 production will somewhat increase the volumetric flow rate along the bed. This change would only slightly rescale the space time variable and therefore would not significantly affect the relative rates of the reforming reactions. To simplify matters, we invoke the constant molar volume assumption (more on this later). For a homogeneous plug-flow reactor free of mass transfer effects, the pseudo-first-order rate constants can be estimated from a nonlinear least-squares fit with

$$d\boldsymbol{c}/d\tau = -\boldsymbol{K}\mathbf{c}, \qquad [1]$$

where $\boldsymbol{c}$ is the concentration vector comprising all hydrocarbon species shown in Fig. 9, $\boldsymbol{K}$ the rate constant matrix, and τ the space time. The explicit forms of $\boldsymbol{c}$ and $\boldsymbol{K}$ will be shown later in the section on modeling of the effect of coke buildup on reactor performance.

Note that if one uses the Langmuir–Hinshelwood rate expression and the data in early works (7–9, 13, 16), one finds that the adsorption denominator is close to unity and varies by less than 5% in our experiments even over the largest difference in space times (0 and 30 min). For most runs it is within the reproducibility tolerance.

We now use the experimental data to evaluate the rate constants at each of five different temperatures. The

approach taken here is to consider the proposed reforming network under the conditions of each of the differential reactor runs and, for each, dissect out the subnetwork that is operative in that experiment. In this way we can estimate the majority of the rate constants somewhat independently. As discussed earlier, k_6 and k_7 are amenable to direct determination from differential reactor experiments such as the one in Fig. 5. This procedure assumes that the rate constants for reactions of ECP are representative of those of all C5Ns, which was experimentally substantiated in (2). Moreover, the mass balance of toluene argument discussed previously yields a good initial estimation of k_2 based on the data obtained by feeding $n\mathrm{C}_7$ to the differential reactor (see Fig. 4).

Next, consider the experiment feeding $i\mathrm{C}_7$ as shown in Fig. 3. After the initial transient, toluene and C5N are present only in negligible concentrations and the major products are $n\mathrm{C}_7$ and light hydrocarbons formed from cracking. Apparently, the $n\mathrm{C}_7$ formed from $i\mathrm{C}_7$ does not have enough time to significantly react further at the high WHSV of 80. Thus the only reactions in the network that are significant in this regime are the isomerization reactions (known to be faster than the other reactions involved such as ring closure) between $i\mathrm{C}_7$ and $n\mathrm{C}_7$ and the cracking of $i\mathrm{C}_7$.

The reduced model and these data give a value for k_4' and at least the ratio of k_3/k_5. Finally, a similar argument (Fig. 4) with $n\mathrm{C}_7/\mathrm{H}_2$ feed yields a value for k_1, an estimate for k_4, and another estimate for k_3/k_5. Before proceeding to the fixed-bed $n\mathrm{C}_7$ feed data, let us summarize: We have good values for k_1, k_6, and k_7 and reasonable estimates, i.e., rather tight bounds on k_2 (determined by feeding $n\mathrm{C}_7$ to the differential microbalance reactor, Fig. 4), the ratio k_3/k_5, k_4 and k_4'. Moreover, we know from Figs. 3 and 4 that k_4 and k_4' are similar in magnitude. This leaves only the magnitude of one of k_3 or k_5 as a totally free parameter, with all others either fixed or free to vary only within narrow bands. We take a conservative approach here, preferring to carry over tight rate constant *bands* from the microbalance differential reactor results to the integral fixed-bed reactor parameter estimation analysis, rather than actual rate constant *values*. The reasons for this caution are as follows. First, the microbalance run is for a particular $i\mathrm{C}_7$. In contrast, the fixed-bed reactor with an $n\mathrm{C}_7$ feed produces a potpourri of $i\mathrm{C}_7$ s, not just 2MH. The rate constants k_5 and k_4' for this mixture, those of interest, should be similar in magnitude to those resulting from the 2MH feed, although not necessarily identical. Finally, the microbalance is only capable of running at a total pressure of 207 kPa as compared to the more relevant value of 517 kPa in the fixed bed. Thus, the theoretical accounting of how the total pressure affects species concentrations and the assumed uniform rate constant–denominator values may be incomplete.

To obtain maximum-likelihood estimates of the remaining parameters, we use a nonlinear least-squares algorithm that adapts a modified Gauss–Newton method, which minimizes the weighted sum of squares and the cross products of the residuals between observed and calculated conversions. At the beginning of the parameter evaluation, we did not assume the same reaction rate constant values (k_4 and k_4') for $n\mathrm{C}_7$ and $i\mathrm{C}_7$ cracking. However, even with different initial guesses for the two rate constants, the nonlinear least-squares fit consistently generated almost identical final values for the two. At lower temperatures, this may be the result of k_3 and k_5 being about a factor of 5 larger than k_4 and k_4' so that the two C_7 isomers interchange fast enough that one measures only the decay rate of $n\mathrm{C}_7$ plus $i\mathrm{C}_7$ as an aggregate. This argument becomes less plausible at the higher temperatures, where k_3 and k_5 are only about twice k_4. Despite this, the quasiequilibrium between $n\mathrm{C}_7$ and $i\mathrm{C}_7$ may still be a good approximation for practical purposes. Hence, to reduce the number of adjustable parameters, we refitted the data assuming identical cracking constants $k_4 = k_4'$, leaving 7, rather than Clem's 14 parameters (6). Of these 7, only 1 is truly free, and the others have good initial guesses and tightly banded values.

Figures 1 and 2 exemplify the agreement between theory and experiment. The model (solid curves) fits the data quite well. Table 2 lists the resulting reaction rate constants for five temperatures. Figure 10 shows the Arrhenius plots for the different rate constants, and Table 2 lists the corresponding apparent activation energies E_i for the ith reaction. The $n\mathrm{C}_7$ dehydrocyclization and cracking have the highest apparent activation energies, while the $n\mathrm{C}_7$ isomerization has the lowest E_i among all the reactions. Also, the apparent activation energies of the reactions $i\mathrm{C}_7 \rightarrow n\mathrm{C}_7$ and $\mathrm{C5N} \rightarrow n\mathrm{C}_7$ are comparable and are much lower than those of dehydrocyclization and cracking. Clearly, these apparent activation energies give a reasonable and consistent explanation of the qualitative temperature effects reported

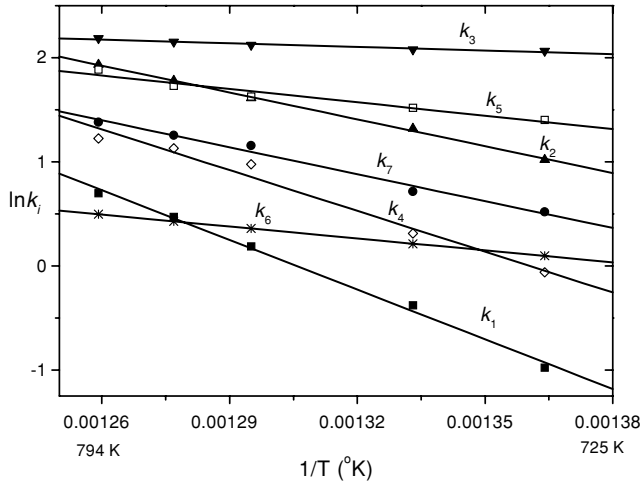

FIG. 10. Arrhenius plots of the different pseudo-first-order rate constants.

TABLE 2

Pseudo-First-Order Rate Constants k_i and Apparent Activation Energies E_i

Temp (°K)	k_i (1/h): Reaction:	k_1 $nC_7 \rightarrow$ C5N	k_2 $nC_7 \rightarrow$ Tol	k_3 $nC_7 \rightarrow iC_7$	k_4 $C_7 \rightarrow C_6^-$	k_5 $iC_7 \rightarrow nC_7$	k_6 C5N $\rightarrow nC_7$	k_7 C5N $\rightarrow$ Tol
733		0.376	1.680	7.881	0.939	4.066	1.102	2.769
750		0.685	2.043	7.975	1.367	4.564	1.236	3.729
772		1.207	3.176	8.338	2.653	5.089	1.432	5.013
783		1.600	3.501	8.601	3.089	5.643	1.534	5.920
794		2.010	3.980	8.902	3.400	6.599	1.641	6.896
	E_i (kJ/mol)	132.3	71.7	9.7	108.6	35.7	31.7	71.5

previously (1, 2); i.e., the higher the temperature, the more C5N, toluene, and cracking products produced and, relatively, the less iC_7 formed. Finally, we remark that the pseudo-first-order kinetics implies low surface coverage. As such, the apparent activation energies are lower than the true activation energies for the surface reactions (E_{si}); that is, $E_i = E_{si} - H_i$, where H_i is the heat of chemisorption.

Sensitivity Analysis

We now illustrate how insensitive a model with many undetermined parameters is when fitting with only experimental (integral) fixed-bed data. Consider the $k_2 \equiv 0$ case, i.e., without the direct six-membered ring closure of nC_7 to toluene. Also, assume there is no direct nC_7 cracking. If one uses only the fixed bed and ignores the microbalance data, the nonlinear least-squares fit finds another set of k's, completely different from those in Table 2, to fit the data. Indeed, at 750°K these k values with the corresponding kinetics model provide a good fit of this limited data set. But the new k_6 (15.7 h^{-1}) and k_7 (40.3 h^{-1}) are much larger than those obtained from the ECP-feed differential microbalance reactor data. Moreover, the reactions C5N $\rightarrow nC_7$ and C5N $\rightarrow$ Tol become much faster than the isomeriaztion reactions $nC_7 \leftrightarrow iC_7$ (new $k_3 = 8.75\ h^{-1}$ and $k_5 = 3.46\ h^{-1}$), which is unreasonable on chemical grounds. Also, such fits likely give negative activation energies for the same reactions. Clearly such comparisons for limited experimental data hardly discriminate among kinetics models. This illustrates the danger of inputting a reaction network with many free parameters into a parameter-estimation program to fit integral reactor data without first doing a series of experiments specifically designed to test the existence and importance of each constituent reaction.

Thus, experiments that only feed pure nC_7, no matter whether they are differential and/or integral ones, are insufficient for the development of a robust reaction scheme and kinetics model. Though such kinetics models might correctly predict the experimental data in a limited range, extrapolation to other experimental conditions is dangerous and interpretation of the rate constants is suspect. Only by measuring different reaction steps separately and combining the differential and integral methods of experiment and analysis, might one arrive at a robust model for the full range of operating conditions of interest. We next further test the adequacy of the model via thermodynamics considerations.

THERMODYNAMICS

The reaction scheme includes the reversible reactions $nC_7 \leftrightarrow iC_7$ and $nC_7 \leftrightarrow$ C5N. An independent check of the rate constants is to compare their values with the equilibrium constant estimated from the free-energy ΔG values based on API-44 data (17). Table 3 compares the equilibrium constants measured at different temperatures in this study to their literature values. The agreement is very good. We note that equilibrium constants estimated from the TRC Thermodynamics Tables (Thermodynamics Research Center, Texas A&M University System) also agree well with those listed in Table 3. This consistency test further suggests that our model and its kinetics parameters form an adequate representation of the reforming kinetics under the conditions employed.

SPATIAL AND TEMPORAL VARIATIONS OF CATALYST COKE AND PRODUCT COMPOSITION

The philosophy of our research has been that the chemistry and kinetics of both the main reaction and the coking reactions are intimately connected and that an adequate understanding of one requires deciphering how the other interacts with it. In particular, to understand the reforming reactions properly, one should be able to account for how the rates of its major reactions change over the long time scale characteristic of catalyst deactivation. To claim to understand the coking, one should also be able to predict coke profiles as functions of on-stream time and of bed position based upon the knowledge of the precursor profile, either measured or predicted. Here, we tie all this together by combining the reforming kinetics with our coking kinetics model from (2) to address both of these expectations. For completeness, we first give a brief account of these catalyst coking kinetics.

TABLE 3

Measured Equilibrium Constants versus those Calculated from Thermodynamics

$K_{ij} = k_i/k_j$ (temperature °K)	K_{16}		K_{35}	
	This work	Thermodynamics	This work	Thermodynamics
733	0.341	0.297 (1C2DMCP)	1.938	1.539 (2MH)[a] 1.518(3MH)[a]
750	0.554	0.576[b]	1.747	1.504 (2MH) 1.500 (3MH)
772	0.843	0.748[b]	1.639	1.461 (2MH) 1.469 (3MH)
783	1.043	1.144 (1C3DMCP)	1.524	1.441 (3MH)
794	1.225	1.289 (1C3DMCP)	1.349	1.422 (2MH) 1.445 (3MH)

[a] 2MH, 2-methylhexane; 3MH, 3-methylhexane.
[b] Average value of 1-*cis*-2-dimethylpentane (1C2DMCP) and 1-*cis*-3-dimethylpentane (1C3DMCP).

Kinetics of Catalyst Coking

As detailed in (2), the coking kinetics model is based on the premise that site coverage is the sole cause of catalyst deactivation. The sequence of events postulated in the model that leads to coke laydown is that a small protocoke molecule forms on an active site. Rather than automatically depositing itself there, it samples both uncoked and coked sites and then deposits *randomly* on one of them and quickly polymerizes there. Let S_0 and S be the active site densities at time zero and t, respectively, and C_k be the coke concentration on the catalyst. A pseudo-steady-state assumption for the protocoke species leads to

$$\frac{dS}{dt} = -\alpha S \frac{dC_k}{dt}, \qquad [2]$$

where α is a units conversion factor divided by S_0. Since the coke production (dC_k/dt) is the product of its clean-catalyst value $r_0(\boldsymbol{c})$ and the fraction ϕ of sites that are active, Eq. [2] integrates to

$$\phi = S/S_0 = \exp(-\alpha C_k) = \left(1 + \alpha \int_0^t r_0(t')\, dt'\right)^{-1}, \qquad [3]$$

which for time-invariant gas concentrations (as in the microbalance) is a hyperbolic decay of active sites with time.

This simple model lends itself naturally to the distinction of coke depositing on clean sites (monolayer coke) and coke depositing on already coked sites (multilayer coke). The total coke concentration is the sum of the monolayer and multilayer coke concentrations. Physically, $1/\alpha$ corresponds to the coke level for a complete monolayer coverage of the active sites (excluding those sites that are lost during the initial hydrocarbon adsorption and coking of the most active sites not included in S_0). For the catalyst here and in [2], the value of α is 56.8 g catalyst/g coke. As shown there, the actual monolayer coke coverage is never complete in a finite time, but rather equals $[(1 - \exp(-\alpha C_k)]/\alpha$. At the same time multilayer coke formation accelerates. After a significant portion of the active sites are coked, the rate of multilayer coke buildup slows down.

The deleterious effect of coke formation on its reaction rate r is generally represented by $r = r_o\phi = r_o \exp(-\alpha C_k)$, where r_o is its initial, coke-free rate. One sees that the damaging marginal effect of coke becomes increasingly weaker with increasing C_k, consistent with the multilayer coke buildup mechanism. Analysis of the data obtained from the vibrational microbalance and the corresponding model in [2] leads to

$$r_c = r_0\phi = (\kappa_1 + \kappa_2/P_H)\frac{P_{C5N}}{P_H}\exp(-\alpha C_k), \qquad [4]$$

relating the coking rate r_c to instantaneous partial pressures of C5N and H_2, and coke-on-catalyst, where r_0 is the initial coking rate. The two deactivation rate constants κ_1 and κ_2 are functions of the initial acid and metal site densities, adsorption equilibrium constants, and polymerization initiation rate constant [2]. At 750° K, $\kappa_1 = 0.016 \pm 0.004$ g coke/(g catalyst · h) and $\kappa_2 = 5.65 \pm 0.69$ g coke kPa/(g catalyst · h). Equation [4] demonstrates that coke slows down its own formation rate, as it should.

Effect of Coke on Reforming Reactions

We now turn to the deactivation of the reforming reactions due to coke buildup. In principle, as the coke-on-catalyst increases, there is no *a priori* reason why all reactions occurring on the bifunctional catalyst should be equally affected. After all, that selectivity changes as a catalyst deactivates is not uncommon in heterogeneous catalysis. Accepting this proposition, one can capture the salient features of the deactivation process by focusing on only

those reactions that are most sensitive to coke. To simplify matters, we divide the reactions into two types: those that are strongly affected by coke and those that are weakly dependent on coke. If the difference in coke sensitivity of these two reaction types is sufficiently large, one can avoid the introduction of new adjustable parameters by simply letting the coke dependence of type 1 reactions be equal and neglecting the coke dependence of type 2 reactions. To switch off the coke dependence of some reactions we introduce a switching constant δ_i such that the rate of the ith reaction in the network takes the form

$$r_i(\tau, t) = r_{io}(\tau)\varphi_i(t) \equiv r_{io}\exp(-\alpha C_k\delta_i) \quad i = 1, 2, \ldots, 7, \qquad [5]$$

where r_{io} is the initial (coke-free) rate, t the on-stream time, $\varphi_i = \phi^{\delta i}$, and $\delta_i = 1$ or 0, depending on whether or not the ith reaction is sensitive to coke. With Eq. [5] and the reforming network shown in Fig. 9, one can construct a model of the reformer's long-term performance, as discussed in the following.

Reactor Model

Let $\boldsymbol{c}^t \equiv (P, I, N, L, T)$, where P, I, N, L, and T are the mole fractions of n-heptane, isoheptanes, C5N, light products from cracking, and toluene, respectively. The governing mass balance equations under the quasi-steady-state assumption are

$$\frac{\partial P}{\partial \tau} = -\sum_{i=1}^{4} k_i\varphi_i P + k_5\varphi_5 I + k_6\varphi_6 N \qquad [6]$$

$$\frac{\partial I}{\partial \tau} = k_3\varphi_3 P - (k_4\varphi_4 + k_5\varphi_5)I \qquad [7]$$

$$\frac{\partial N}{\partial \tau} = k_1\varphi_1 P - (k_6\varphi_6 + k_7\varphi_7)N \qquad [8]$$

$$\frac{\partial T}{\partial \tau} = k_2\varphi_2 P + k_7\varphi_7 N \qquad [9]$$

$$\frac{\partial L}{\partial \tau} = k_4\varphi_4(P + I) \qquad [10]$$

$$\frac{\partial C_k}{\partial t} = (\kappa_{10} + \kappa_{20}/P_H)P_{C5N}\phi/P_H. \qquad [11]$$

The boundary ($\tau = 0$) and initial ($t = t_o$) conditions are

$$\tau = 0, \quad P = 1, \quad I = N = T = L = C_k = 0 \qquad [12]$$

for all t, and

$$t = t_o, \quad C_k = C_{ko}(\tau), \quad P = P_o(\tau), \quad I = I_o(\tau), \quad N = N_o(\tau), \quad T = T_o(\tau), \quad L = L_o(\tau) \qquad [13]$$

for all τ. These equations upon integration predict $\boldsymbol{c}(\tau, t)$ and $C_k(\tau, t)$, which would provide a very stringent test of the theory for two main reasons. First, all the rate constants are predetermined and therefore not adjustable. Second, we use the coking rate constants determined at low P_H and P_H/P_{C5N} to predict coke profiles at high P_H and P_H/P_{C5N}. Recall that κ_1 and κ_2 were determined from both reformer and vibrational microbalance data, where the latter reactor operated at a P_H and P_H/P_{C5N} much lower than that in the integral reactor where the reforming kinetics are measured. So the microbalance produces a much higher coke at shorter on-stream times compared to the integral reactor. In the absence of a reforming kinetics model that contains C5N as a kinetic lump and predicts its spatiotemporal evolution, our previous attempts (1, 2) at predicting $C_k(\tau, t)$ were simply empirical and heuristic.

Before performing the integration, we need to discuss the initial condition $t = t_o$. As reported previously (1, 2), the vibrational microbalance data show that there is an almost instantaneous coke buildup of about 0.6 wt% upon introduction of the n-heptane feed into the microbalance. We thus need to account for this "instantaneous" coke laydown for the integral reactor as well. After this initial sharp rise, there is still a further increase in C_k during the ~30-h reactor start-up period, after which the k_i are determined. Using the k_i values listed in Table 2, we can readily obtain analytical expressions for $P_o(\tau)$, $I_o(\tau)$, $N_o(\tau)$, $T_o(\tau)$, and $L_o(\tau)$ corresponding to $t = t_o = 30$ h. To march on the integration for $t > 30$ h, however, we need to know the reactor coke profile $C_{ko}(\tau)$ at $t_o = 30$ h. This is estimated as follows. We integrate Eqs. [6] to [13] from $t = 0$ up to $t = 30$ h by imposing the following initial condition at $t = 0$: $C_k = 0.6$ wt% and $P = P_o(\tau)$, $I = I_o(\tau)$, $N = N_o(\tau)$, $T = T_o(\tau)$, and $L = L_o(\tau)$. The assumption here is that within the 30-h start-up period C_k does not significantly affect the hydrocarbon concentrations. With the thus-obtained $C_{ko}(\tau)$ at $t_o = 30$ h, we then integrate Eqs. [6] to [13] again to calculate P, I, N, T, L, and C_k for $t > 30$ h at any τ. The results are not sensitive to the value assigned to t_o; for instance, the two cases $t_o = 30$ and 40 h give essentially the same results. The numerical method used for integrating Eqs. [6] to [11] is a second-order finite difference scheme with a mesh size ratio $\Delta\tau/\Delta t$ that avoids numerical instabilities.

As alluded to earlier, we invoke the constant molar flow rate assumption in estimating the rate constants k_i. However, this assumption needs to be relaxed to calculate C_k accurately. One reason is that even a small gas dilution, due to the production of light hydrocarbons (C_6^-) and H_2, can have a noticeable effect on the partial pressure of the minute amount of C5N present. Another reason is that the coking rate is sensitive to P_H, although P_H increases slightly in the reactor's downstream. These effects might cause a rapid decline in C_k away from the reactor inlet region. Thus, in calculating C_k at each grid point (τ, t), we also estimate the extents of C5N dilution and H_2 production stoichiometrically by assuming that the cracked products are from

the primary cracking only and correct their concentrations for these effects. This assumption is defensible because the effect due to the H_2-consuming secondary cracking is small.

The method of solution described earlier is repeated for different sets of $\{\delta_i\}$ values to find the best match between theory and experiment. In addition, the final $\{\delta_i\}$ chosen must be mechanistically reasonable on chemical grounds, as we discuss later.

Since the majority of catalyst life data are obtained at 750°K and 517 kPa, we will test the reforming and coking models against the product composition and coke profile data collected under these conditions. With the k_i values listed in Table 2 for 750°K, we integrate Eqs. [6] to [10] analytically to give

$$P_o = 0.7250e^{-\lambda_1\tau} + 0.2742e^{-\lambda_2\tau} + 0.0008e^{-\lambda_3\tau} \quad [14]$$

$$I_o = -0.585e^{-\lambda_1\tau} + 0.578e^{-\lambda_2\tau} + 0.007e^{-\lambda_3\tau} \quad [15]$$

$$N_o = -0.0457e^{-\lambda_1\tau} + 0.0668e^{-\lambda_2\tau} - 0.0211e^{-\lambda_3\tau} \quad [16]$$

$$T_o = 0.4433 - 0.0828e^{-\lambda_1\tau} - 0.3769e^{-\lambda_2\tau} + 0.0154e^{-\lambda_3\tau} \quad [17]$$

$$L_o = 0.5567 - 0.0121e^{-\lambda_1\tau} - 0.5425e^{-\lambda_2\tau} - 0.0021e^{-\lambda_3\tau}, \quad [18]$$

where the three eigenvalues are $\lambda_1 = 15.826$, $\lambda_2 = 2.147$, and $\lambda_3 = 4.997$ (1/h). The system has three characteristic time scales. The fastest, characterized by $1/\lambda_1$, is dominated by the isomerization, dehydrogenation, and ring expansion reactions. The slowest, characterized by $1/\lambda_3$, is dominated by the cyclization and ring opening/closure reactions.

Comparison of Theory and Experiment

The data used for comparison are C_k at $t = 224$ and 240 h and $\boldsymbol{c}$ at $t = 70$, 100, and 130 h. Since the movement of the coke profile is so slow, the data for $t = 224$ and 240 h can be safely grouped together.

Figure 11, a snapshot of the state of catalyst coking in the integral reactor, shows the predicted and measured coke profiles along the bed. The predicted coke level is calculated for t up to the 240th h. The dashed line corresponds to the case where all reactions are deactivated by coke, that is, uniform deactivation with $\delta_i = 1$ for all i. This case does not even give the correct trend, suggesting that the deactivation is a selective phenomenon. Compared to the model prediction, the data show a faster coke buildup near the reactor entrance followed by a faster decline away from the reactor inlet region. What is going on is the chemistry initially sets up a C5N profile with a maximum about 1/4 down the reactor and decaying beyond. Since the coking rate is linear in C5N, the catalyst cokes fastest at this maximum, the reactions slow down there and move the maximum downstream. This process continues until the C5N maximum exits the reactor. From that point on the

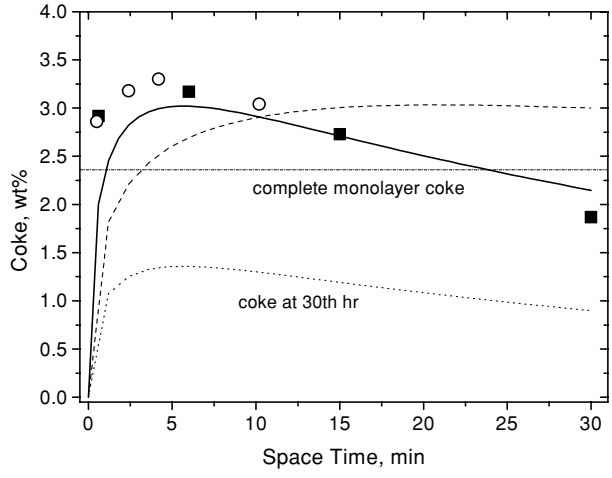

FIG. 11. Coke profiles along the reactor using nC_7 as feed; 750°K and 517 kPa; dashed line, uniform deactivation for $t = 240$ h ($\delta_i = 1$ for all i); solid line, selective deactivation for $t = 240$ h ($\delta_1 = \delta_2 = \delta_6 = 1$, $\delta_i = 0$ for all other i); dotted line, selective deactivation for $t = 30$ h; horizontal line, complete monolayer coke coverage.

C5N profile, and thus the instantaneous coke buildup, is monotonically increasing along the bed, resulting at 240 h in an aggregate profile without a maximum. To portray the observed behavior, given the fact that C5N concentration is the main driver for coke production, reaction 7, that depletes C5N and whose deactivation causes the C5N maximum to move downstream, must be coke-insensitive. For chemical sensibility (see below) one may pick the selective deactivation case with $\delta_1 = \delta_2 = \delta_6 = 1$, $\delta_i = 0$ for all other i. Among the three deactivating reactions, the fastest one, measured by k_2, is hurt more than the slow ones (k_1 and k_6). This will free up some nC_7 which would help to offset the coking of reaction 1 which produces C5N in the reactor's upstream. The C5N-to-toluene reaction (k_7), being free of catalyst deactivation, will create a strong drainage for C5N, thereby causing a sharp decline of the C5N concentration in the reactor's downstream, thus giving a steep decline in the cumulative coke made in the reactor's downstream.

Indeed, by setting $\delta_1 = \delta_2 = \delta_6 = 1$, and $\delta_i = 0$ for all other i, we obtain the solid line that predicts the data very well. Note that the measured coke level near the reactor entrance (Section 1, Table 1) is much higher than that predicted from the model. The very high coke level in Section 1 is most likely caused by the contamination with the high-coke-content catalyst which dropped into Section 1 during catalyst unloading (see Liu *et al.* (2) for details). We should also remark that the coke profile shown in Fig. 11 is quite different from that reported in Refs. (9) and (16), which considered only 10 h of coking.

We further test this choice ($\delta_1 = \delta_2 = \delta_6 = 1$, $\delta_i = 0$ for all other i) to see if it can correctly predict $\boldsymbol{c}(\tau, t)$ for $t = 70$, 100, and 130 h. Figures 12 and 13 show the concentrations of n-heptanes, isoheptanes, toluene, and C_1–C_6 cracked

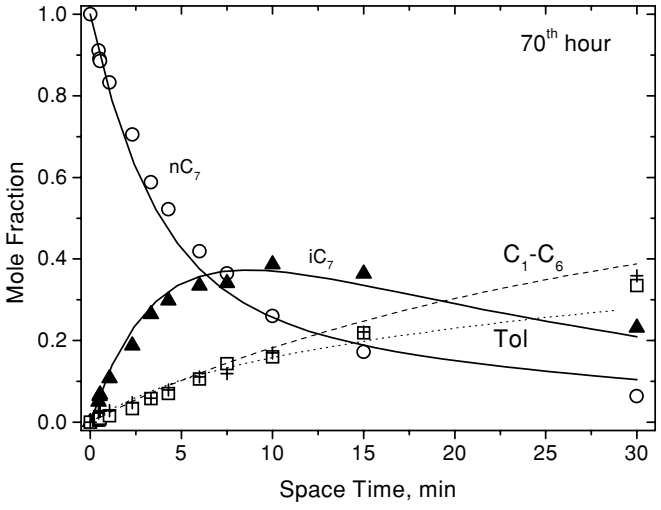

FIG. 12. Mole fractions of *n*-heptane, isoheptanes, toluene (□) and C_1–C_6 cracking products (+); $t = 70$ h, 750°K and 517 kPa.

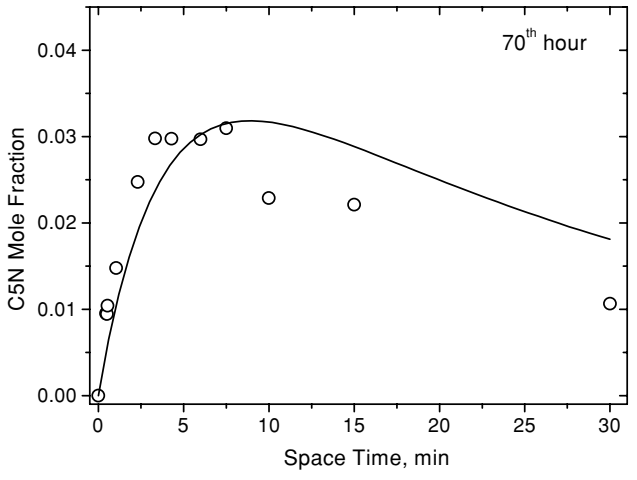

FIG. 14. Mole fraction of five-membered naphthenes for $t = 70$ h; 750°K, 517 kPa.

products for $t = 70$ and 130 h, respectively. The agreements are good. We do not show the results for the 100th hour because they are very similar to those for the 70th and 130th hours. A more severe test is the prediction of the C5N concentration whose very low values are susceptible to large errors. As Figs. 14 ($t = 70$ h) and 15($t = 130$ h) show, the model does a good job in this respect.

We tried many other different combinations of δ_i values, none of which gives a better fit than the earlier case. The C5N and coke reactor profiles are more sensitive tools for discriminating among different combinations of δ_i values.

We now extrapolate this model to the reactor start-up period. Figure 11 also shows the predicted coke profile (dotted line) at the 30th h, which is far below the level of $0.6 + 1/\alpha = 2.36$ wt% (the horizontal line) for complete monolayer coverage. Thus, a significant portion of the active sites is still available for reforming after 30 h on stream. In contrast, the conditions used in the microbalance experiments are so much more severe that essentially a complete monolayer coke level is reached after 30 h even at a much lower temperature of 717°K (2).

To sum up, the combination of our new reforming kinetics and catalyst coking models, when allowing for selective deactivation, predicts both the temporal and the spatial evolution of all the reaction participants, including the coke, very well. This provides us with considerable insight into the manner in which the catalyst deactivates. One can use the present models for many simulation purposes. Figure 16 is a three-dimensional plot of the spatial and temporal variation of C_k at 750°K and 517 kPa for t up to 240 h.

Some remarks on the practical implications of the foregoing results are in order. Since the formation of toluene from C5N does not appear to be sensitive to coke, one would expect that two feeds with different paraffins/naphthenes

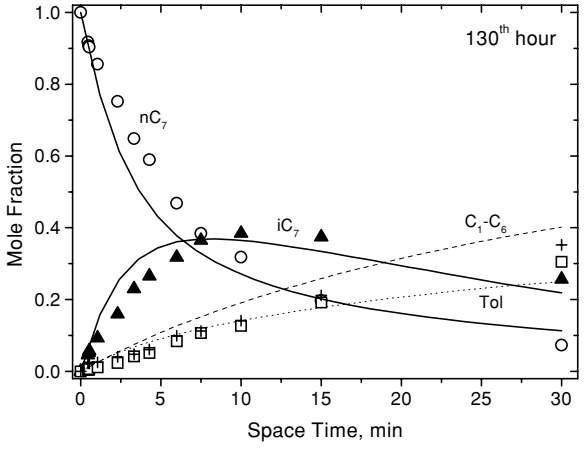

FIG. 13. Mole fractions of *n*-heptane, isoheptanes, toluene (□), and C_1–C_6 cracking products (+); $t = 130$ h; 750°K and 517 kPa.

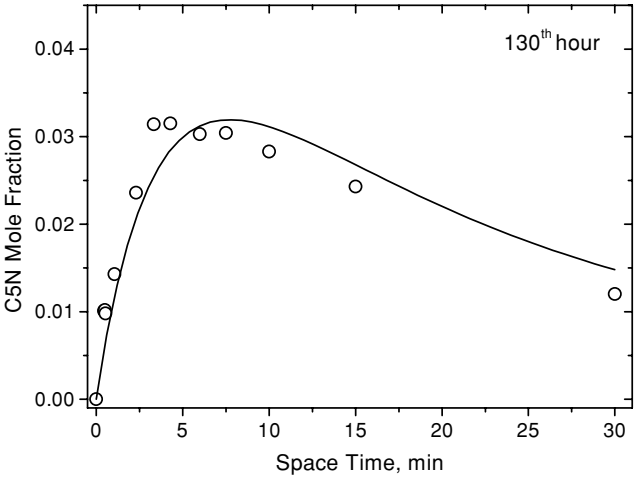

FIG. 15. Mole fraction of five-membered naphthenes for $t = 130$ h; 750°K, 517 kPa.

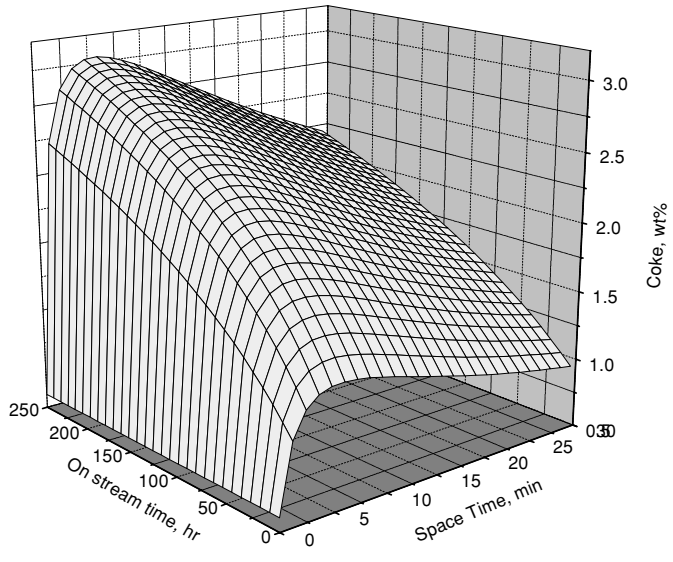

FIG. 16. Spatial and temporal variations of coke profile in reactor; 750°K, 517 kPa.

ratios would exhibit quite different on-stream behaviors. The lumped reforming network and its relation to catalyst coking can be used for the development of process models for commercial reforming feedstocks. It can also be used for feed selection and blending. Joshi *et al.* (18) applied graph theory to build the naphtha reforming model from rate data on pure compounds.

On the fundamental side, the foregoing development explains why the Pt–Ir/Al_2O_3 catalyst is more active and stable than the Pt–Re/Al_2O_3 catalyst reported by Carter *et al.* (19). They proposed that the high hydrogenolysis activity of Ir helps to remove coke (and/or its precursors) from metal surfaces, thus mitigating the deactivation effect on paraffin ring closure reactions (i.e., k_1, k_2, and k_6). The key message of all this is that our results for the first time quantitatively point to the importance of selective deactivation by coke, a phenomenon that deserves further investigation. In the following, we propose a possible physical picture of its origin.

Nature of Selective Deactivation by Coke

The question at hand is, why do some reactions in the network appear to be much more sensitive to coke than other reactions? A short answer is that the high sensitivity probably arises from the specific active site requirements demanded by those highly sensitive reactions.

To give a physical explanation of the selective deactivation, we draw an analogy with the Ni–Cu bimetallic catalyst system studied by Sinfelt *et al.* (20, 21). For ethane hydrogenolysis, they observed that the addition of only a small amount of inactive Cu atoms substantially decreased the catalyst activity. Their interpretation is that the surface intermediates require bonding of carbon atoms to multiplets of adjacent Ni atoms. Geometrically, one can see that it does not take much Cu to break up the multiplets, which explains the deactivation effect of Cu. In the case of cyclohexane dehydrogenation, by contrast, Cu has little, if any, effect on the activity of Ni. Here the reaction, being much less demanding than the hydrogenolysis reaction (C–C bond rupture), does not require a multiplet of Ni sites.

The foregoing geometric effect can be carried over to our system if we view coke as playing the role of Cu. We thus proceed to propose that the formation or breaking of a ring compound (k_1, k_6, and k_2), the heart of reforming reactions, requires a multiplet of metal atoms. As such, even a small amount of coke can drastically reduce the concentration of these multiplets. This should also be the case with the metal hydrogenolysis activity. However, its contribution to the formation of C_1–C_6 light products diminishes significantly after the initial ~30-h lineout period. In other words, the k_4 value we measured essentially reflects acid cracking. On the other hand, it is reasonable to propose that hydrogenation, dehydrogenation, isomerization, ring expansion, and acid cracking (k_7, k_3, k_5, and k_4) do not require multiplets and they become relatively stable after the lineout period.

The foregoing argument helps to explain the results borne out from our modeling study. The essential point here is that just because coke can indiscriminately deposit on the catalyst surface does not mean that all reactions are affected equally. This reaction-sensitive deactivation phenomenon is consistent with the fact that a paraffinic feed requires a higher reforming temperature and more frequent catalyst regeneration than a naphthenic feed. As coke builds up on the catalyst, the aromatization of naphthenes remains unaffected, whereas the aromatization of paraffins slows down due to decrease in k_1, k_2, and k_6. This in turn requires an increase in the reformer temperature to maintain constant product octane. A higher temperature increases the coking rate, thereby further lowering paraffin aromatization. When the reformer reaches the maximum permissible temperature, the catalyst is regenerated. Monitoring changes in k_1, k_2, and k_6 may improve reformer performance through optimization of the catalyst regeneration schedule.

CONCLUSIONS

We have developed a lumped reaction network and its corresponding kinetics model for *n*-heptane reforming over an unsulfided Pt–Re/Al_2O_3 catalyst by combining both the differential and the integral methods of analysis. The resulting reforming kinetics model, when used along with previously developed coking kinetics model, provides us with a powerful tool for *a priori* predictions of the evolution of catalyst coke profiles and a reforming product composition as a function of on-stream time, bed position, and operating conditions. This has a direct bearing on the simulation of both the reforming reaction process and its

catalyst regeneration process, since the coke profile is an initial condition for the control and optimization of the catalyst's regeneration process.

Our modeling study indicates that while coke can indiscriminately deposit on different active sites and on already formed coke, its influence on the rates of various reactions in the reforming network can be quite selective. This is a very important consideration in both catalyst design and process development. Further work in this area is needed; for instance, it is definitely worthwhile to probe the genesis of the apparent selective catalyst deactivation. Finally, the present experimental and modeling protocol for investigating catalyst deactivation can also be extended to catalytic systems other than reforming.

APPENDIX: NOMENCLATURE

$\boldsymbol{c}$	concentration vector $\boldsymbol{c}^t = (P, I, N, L, T)$
C_k	total amount of coke on catalyst, g coke/g catalyst
C5N	five-membered naphthenes
C6N	six-membered naphthenes
C_6^-	cracking products of nC_7 reforming
E_i	apparent activation energy of the ith reaction, kJ/mol
ECP	ethylcyclopentane
H_i	heat of chemisorption for the ith reaction
I	mole fraction of iso-heptanes
iC_7	iso-heptane
k_i	pseudo-first-order reaction constants, $i = 1, 2, \ldots, 7$; 1/h
L	mole fraction of light products from cracking
MCP	methylcyclopentane
MCH	methylcyclohexane
MH	methylhexane
N	mole fraction of C5N
nC_7	normal heptane
P	mole fraction of n-heptane
P_H	partial pressure of H_2, kPa
P_{C5N}	partial pressure of coke precursor C5N, kPa
S	density of active sites on catalyst
S_o	initial density of active sites on catalyst
r_{co}	initial rate of coke formation, g coke/g catalyst h
r_c	rate of coke formation, g coke/g catalyst h
t	on-stream time, h
T	mole fraction of toluene
TOL	toluene
WHSV	weight-hourly space velocity (g feed/(g catalyst · h))

Greek Letters

α	deactivation constant, g catalyst/g coke
δ_i	defined in Eq. [5], $i = 1, 2, \ldots, 7$
φ_i	reaction-specific deactivation function, $i = 1, 2, \ldots, 7$
ϕ	deactivation function
λ_i	eigenvalues, $i = 1, 2, 3$
κ_1	coking reaction rate constant of alkylcyclopentene
κ_2	coking reaction rate constant of alkylcyclopentadine
τ	space time

ACKNOWLEDGMENT

Thanks are due to Dr. J. H. Sinfelt, who drew our attention to the selective deactivation phenomenon observed with the Ni–Cu catalyst system.

REFERENCES

1. Liu, K., Fung, S. C., Ho, T. C., and Rumschitzki, D. R., *J. Catal.* **169**, 455 (1997).
2. Liu, K., Fung, S. C., Ho, T. C., and Rumschitzki, D. R., *Ind. Eng. Chem. Res.* **36**, 3264 (1997).
3. Kugelmans, A. M., *Hydrocarb. Proc.* January, 95 (1976).
4. McHenry, K. W., Bertolacini, R. J., Brennan, H. M., Wilson, J. L., and Seelig, H. S., *in* "Proceedings, 2nd International Congress on Catalysis, Paris, 1960," No. 117, p. 1, Technip, Paris, 1961.
5. Mahoney, J. A., *J. Catal.* **32**, 247 (1974).
6. Clem, K. R., Ph.D. dissertation, Louisiana State University, Baton Rouge, Louisiana, 1977.
7. Van Trimpont, P. A., Marin, G. B., and Froment, G. F., *Appl. Catal.* **24**, 53 (1986).
8. Van Trimpont, P. A., Marin, G. B., and Froment, G. F., *Ind. Eng. Chem. Fund.* **25**, 544 (1986).
9. Van Trimpont, P. A., Marin, G. B., and Froment, G. F., *Ind. Eng. Chem. Res.* **27**, 51 (1988).
10. Sun, S. Z., Weng, H. X., Mao, X. J., and Liu, F. Y., *Chem. React. Eng. Technol.* **8**, 10 (1992).
11. Sun, S. Z., Weng, H. X., Mao, X. J., and Liu, F. Y., *Chem. React. Eng. Technol.* **8**, 18 (1992).
12. Ramage, M. P., Graziani, K. R., and Krambeck, F. J., *Chem. Eng. Sci.* **35**, 41 (1980).
13. Ramage, M. P., Graziani, K. R., Schipper, P. H., Krambeck, F. J., and Choi, B. C., *Adv. Chem. Eng.* **13**, 193 (1987).
14. Querini, C. A., and Fung, S. C., *J. Catal.* **141**, 389 (1993).
15. Fung, S. C., and Querini, C. A., *J. Catal.* **138**, 240 (1992).
16. Marin, G. B., and Froment, G., F., *Chem. Eng. Sci.* **37**, 759 (1982).
17. Rossini, F. D., *et al.*, "Selected Values of Physical and Thermodynamic Properties of Hydrocarbons and Related Compounds," Carnegie Press, Pittsburgh, PA (1953).
18. Joshi, P. V., Klein, M. T., Huebner, A. L., and Leyerle, R. W., *Rev. Proc. Chem. Eng.* **2**, 169 (1999).
19. Carter, J. L., McVicker, G. B., Weissman, W., Kmak, W. S., and Sinfelt, J. H., *Appl.Catal.* **3**, 327 (1982).
20. Sinfelt, J. H., Carter, J. L., and Yates, D. J. C., *J. Catal.* **24**, 283 (1972).
21. Sinfelt J. H., "Bimetallic Catalysts: Discoveries, Concepts, and Application." Wiley, New York, 1983.